frontiers | Frontiers in Earth Science

TYPE Original Research
PUBLISHED 30 August 2022
DOI 10.3389/feart.2022.993074

OPEN ACCESS

EDITED BY
Kevin Cheung,
E3-Complexity Consultant, Australia

REVIEWED BY
Haibo Bi,
Institute of Oceanology (CAS), China
Ruibo Lei,
Polar Research Institute of China, China
Aliakbar Rasouli,
University of Tabriz, Iran

*CORRESPONDENCE
Liu Na,
liun@fio.org.cn

SPECIALTY SECTION
This article was submitted to Interdisciplinary Climate Studies, a section of the journal Frontiers in Earth Science

RECEIVED 13 July 2022
ACCEPTED 04 August 2022
PUBLISHED 30 August 2022

CITATION
Xinyuan L, Na L, Lina L, Lei Y, Yunbo L, Long F, Hongxia C, Yingjie W, Bin K, Yuyuan Z and Ning L (2022), Causes of the drastic change in sea ice on the southern northwind ridge in July 2019 and July 2020: From a perspective from atmospheric forcing. *Front. Earth Sci.* 10:993074. doi: 10.3389/feart.2022.993074

Causes of the drastic change in sea ice on the southern northwind ridge in July 2019 and July 2020: From a perspective from atmospheric forcing

Lv Xinyuan[1,2,3], Liu Na[1,2,3]*, Lin Lina[1,2,3], Yang Lei[1,2,3], Li Yunbo[4], Fan Long[5], Chen Hongxia[1,2,3], Wang Yingjie[1,2,3], Kong Bin[1,2,3], Zhang Yuyuan[1,2,3] and Liu Ning[6]

[1]First Institute of Oceanography, Key Laboratory of Marine Science and Numerical Modeling, Ministry of Natural Resources, Qingdao, China, [2]Laboratory for Regional Oceanography and Numerical Modeling, Pilot National Laboratory for Marine Science and Technology, Qingdao, China, [3]Shandong Key Laboratory of Marine Science and Numerical Modeling, Qingdao, China, [4]The 91001 Unit of PLA, Beijing, China, [5]Navy Research Institute, Tianjin, China, [6]College of Underwater Acoustic Engineering, Harbin Engineering University, Harbin, China

Arctic sea ice is a key factor in high–latitude air–sea–ocean interactions. In recent decades, its extent has been decreasing in all seasons with large interannual variability, especially for the Northwind Ridge. After removing the trend in the changes during July 1979 to 2020, 2019 had an abnormally low value, while the following year, 2020, had an abnormally high value. The underlying processes driving this variability in July near the southern Northwind Ridge, which is one of the areas with the most drastic changes in Arctic, are not well understood. There, we demonstrated that the shortwave radiation anomaly in July is the direct reason for the sea ice anomaly in July 2019 and July 2020. Importantly, the total energy surplus in the spring of 2019 (enough to melt ~18 cm of sea ice) and 2020 (potentially melting ~11 cm of sea ice) indirectly influenced the sea ice. The abnormal change in moisture and its convergence mainly caused by atmospheric circulation were the main reasons for the longwave radiation and latent flux anomalies. Cloud water mainly affected shortwave radiation, including the positive net shortwave radiation anomaly in May 2019.

KEYWORDS

sea ice, southern northwind ridge, interannual variation, radiative flux anomalies, turbulent flux anomalies, atmospheric circulation

Introduction

As the area most severely affected by global warming in the world, the sea ice extent in the Arctic has been decreasing steadily during the satellite remote–sensing era from 1979 to present. Changes in the Arctic climate and the loss of Arctic sea ice have considerable influence on climate and extreme weather in China (Wu et al., 2009; Lei et al., 2017b). The pattern of the reduction is not spatially uniform; for example, the Northwind Ridge in the western Canada Basin has experienced a catastrophic decrease in sea ice (Sumata and Shimada, 2007; Mizobata and Shimada, 2012).

Multiple factors have conspired to produce the observed sea ice anomaly, but their relative importance remains unknown. These influencing factors can be roughly divided into thermal and dynamic factors, such as surface air temperature (Curry, Schramm, and Ebert, 1995; Barrientos Velasco, Deneke, Griesche, Seifert, Engelmann, and Macke, 2020), the solar surface radiation budget (Gong, Feldstein, and Lee, 2017; Barrientos Velasco, Deneke, Griesche, Seifert, Engelmann, and Macke, 2020; Liang, Bi, Wang, Zhang, and Huang, 2020), the downward longwave flux (Park, Lee, Son, Feldstein, and Kosaka, 2015; Gong, Feldstein, and Lee, 2017; Liang, Bi, Wang, Zhang, and Huang, 2020), atmospheric circulation, which can transport atmospheric heat poleward in response to wind/pressure patterns (Graversen, Mauritsen, Tjernström, Källén, and Svensson, 2008; Graversen, Mauritsen, Drijfhout, Tjernström, and Mårtensson, 2011), ocean currents (Polyakov, Beszczynska, Carmack, Dmitrenko, Fahrbach, Frolov et al., 2005) and ocean conditions (for example, ocean warming (Polyakov, Timokhov, Alexeev, Bacon, Dmitrenko, Fortier et al., 2010)) (Kapsch, Graversen, and Tjernström, 2013).

Compared with 2019, the spatial distribution characteristics of the sea ice concentration (SIC) in 2020 for the Northwind Ridge moved southward overall (Figure 1). In the southern Northwind Ridge, the SIC in 2019 was mainly below 20%, while in 2020, it was mostly above 60%.

According to the change in the trend of the average SIC for the southern Northwind Ridge from 1979 to July 2020 (Figure 2), 2019 marked the minimum SIC (Figure 2A). Even after removing the trend changes over the past 40 years, SIC in 2019 was still relatively low (Figure 2B). Against the background of declining sea ice in the southern Northwind Ridge, there was an abnormal increase in sea ice in 2020 (Figure 2B). Does this abnormal change in July occur in its adjacent June and throughout the summer (July, August and September)? Comparing the changes in SIC in this area in June shows that the SIC in 2019 and 2020 was above 80% (Supplementary Figure S1). Although this phenomenon was observed in August, it was far weaker than that in July (Supplementary Figure S2), and this abnormal change in 2019 and 2020 was disappeared in September (Supplementary Figure S3).

What caused the dramatic and abnormal decrease of sea ice in the southern Northwind Ridge in July 2019, and why was the July 2020 SIC unusually higher than in previous years? We conduct a comparative analysis of the two abnormal years between 2019 and 2020, including both dynamical and thermodynamical changes, and study the mechanisms and connections from a perspective from atmospheric forcing that caused the abnormal variability during these 2 years.

Previous studies on SIC have mostly focused on changes in the multi–year trend and during September when the ice reaches its annual minimum extent (Kay et al., 2008); however, there is no compelling discussion and conclusion on the cause and mechanism for the variation of sea ice in July. In addition, the southern Northwind Ridge is not only one of the areas with the most drastic changes in Arctic, but also a key sea area for the deployment of mooring systems during the Chinese National Arctic Research Expedition, and the change of SIC directly affects their deployment and recovery. Therefore, it is important to

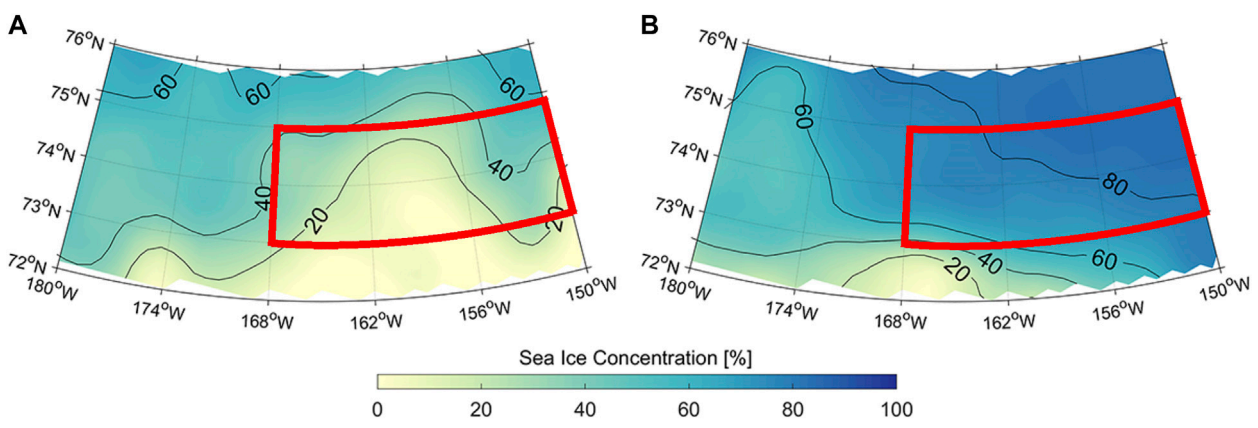

FIGURE 1
SIC in July for 2019 **(A)** and 2020 **(B)**. Red polygons encapsulate areas represents the study area of this paper.

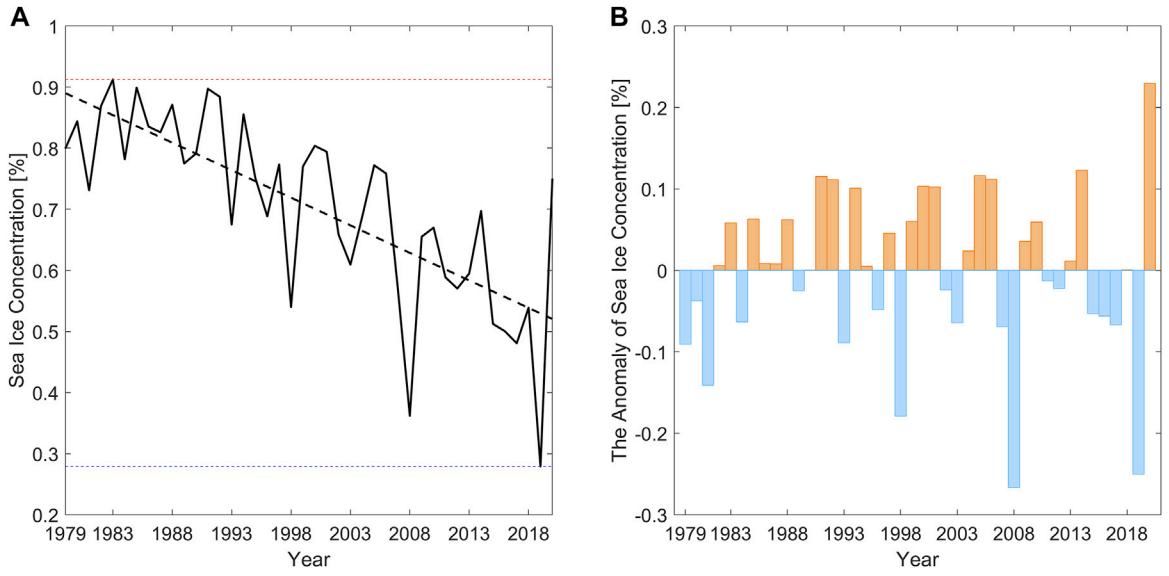

FIGURE 2
Arctic SIC **(A)** and the anomaly of SIC **(B)** for July 1979–2020. The black dotted line is the linear trend. The red dotted line indicates the maximum SIC over the past 40 years, while the blue dotted line indicates the minimum SIC during the same time period.

explore the reasons for the abnormal changes in the SIC here. This study analyzed in depth the reasons from a perspective from atmospheric forcing for the drastic reduction of sea ice in July 2019 and the abnormal increase in sea ice in July 2020 at the southern Northwind Ridge. On this basis, we further explored the main factors that caused the difference between the 2 years.

Materials and methods

Spring in this paper is defined as April to June. We selected the southern Northwind Ridge (73–75°N, 168–150°W) as the study area (red box in Figure 1).

Various atmospheric fields were taken from the ERA5 reanalysis from the European Center of Medium Range Weather Forecast (ECMWF) (Hersbach, Bell, Berrisford, Biavati, Horányi, Muñoz Sabater et al., 2018). The energy transport is vertically integrated from the top to the bottom of the atmosphere (Graversen, 2006). ERA5 is the next version of ERA-Interim (ended in August 2019), with improvements and enhancements of various aspects. For example, sea surface temperature and sea ice in ERA5 are more consistent, and the atmospheric assimilation system has evolved from the Integrated Forecasting System (IFS) Cycle 31r2 to IFS Cycle 47r1 (June 2020) (Haiden, Janousek, Vitart, Ben-Bouallegue, Ferranti, Prates et al., 2021). The credibility of ERA5 in the representation of Arctic climate has not been established but several studies have found that ERA-Interim is one of the best performing reanalysis products (Kapsch, Graversen, and Tjernström, 2013; Danielson, Ahkinga, Ashjian, Basyuk, Cooper, Eisner et al., 2020). It has been shown that the downwelling longwave radiation fluxes from the ERA-Interim reanalysis are more consistent with observations, including for the seasonal cycle, monthly correlations and latitudinal dependence (Shi, Wild, and Lettenmaier, 2010; Cox, Walden, and Rowe, 2012; Zygmuntowska, Mauritsen, Quaas, and Kaleschke, 2012).

We also used the daily gridded data of SIC derived from the Scanning Multichannel Microwave Radiometer (SMMR; 1979–1987), Special Sensor Microwave/Imager (SSM/I; 1987–2006), and Special Sensor Microwave Imager/Sounder (SSMIS; 2005 onward). These data are produced by the European Organisation for the Exploitation of Meteorological Satellites (EUMETSAT) Ocean and Sea Ice Satellite Application Facility (OSI SAF) (data accessed from https://doi.org/10.24381/cds.3cd8b812). The horizontal resolution is the 25 km grid resolution.

The convergence of latent heat transport here is the convergence of water vapor. The drystatic energy transport is defined as the sum of the kinetic energy flux, the thermal energy flux and the geopotential flux, while the latent energy transport can be defined as the total energy flux minus the dry–static energy transport.

We use the following two methods to analyze the time series of net shortwave radiation, net longwave radiation, downward shortwave radiation, downward longwave radiation, sensible flux, latent flux, total column water vapor, total column cloud liquid water, the convergence of dry–static energy and the convergence of latent energy averaged on the southern

Northwind Ridge. Method one: the daily data are detrended based on 1979–2020. Method two: the mean of 1979–2020 for each day is removed. Compared with the traditional method of using the average value, this paper has improved and optimized the approach. First, the daily linear trend during 1979–2020 for each variable is calculated. Then, the average of the daily linear trend is obtained. Finally, the difference is processed to obtain the abnormal time series of each element. By estimating the anomalies relative to the linear trend rather than the mean, the focus is on the year–to–year variability rather than the long–term change (Kapsch, Graversen, and Tjernström, 2013). The anomaly of SIC is obtained using the first method mentioned above.

The anomaly of the mean sea level pressure (MSLP) and 500 hPa geopotential height are removed from the mean field of 1979–2020. We assume that the vertically integrated northward heat flux, the vertically integrated northward water vapor flux and the vertically integrated northward cloud liquid water flux are changed with the change of the pressure field, and therefore, the three fields are treated the same as the pressure field.

Results

To quantify the reduction in ice area, we first focus on the thermodynamical component. The net shortwave radiation (SWN), shortwave radiation downwards (SWSD), longwave radiation (LWN), longwave radiation downwards (LWSD), and turbulent fluxes (sensible hear flux (SH) and latent heat flux (LH)) are analyzed below. Method one (Figure 4 and Figure 5) and two (Supplementary Figure S4 and Supplementary Figure S5) have basically the same trend of the atmospheric variable fields, but the range of method two is larger than that of method one.

The time period that caused the difference in sea ice between July 2019 and July 2020 occurred from mid–to–late June to mid–to–late July (Figure 3). During this time period, the rate of sea ice reduction in 2019 was much faster than that in 2020, which directly affects the time point when the ice–free state will be reached (Figure 3). In 2020, the negative anomaly of SWN appeared in early July, which is largely the same as the occurrence of sea ice anomalies, indicating that solar radiation is one of the reasons for the abnormally high sea ice in July 2020 (Figure 4A). In 2019, SWN occurred abnormally in mid–July, and before that (June to mid–July) SIC fell sharply (Figure 3 and Figure 4A). Moreover, the melting season of 2019 began in mid–to–early May, earlier than early June 2020 (Figure 3). According to Figure 4A, Figure 4C and Figure 4E, the changes in LWN, LH and SH from April to May 2020 are all much smaller than those in 2019. We believe that the heat accumulated by LWN, LH and SH during the spring of 2019 is one of the reasons for 1) the melting season in 2019 occurring earlier than in 2020 and 2) the sharp decrease in SIC before SWN being abnormal. The significant increase in LWN and LH positive anomalies in June 2020 is the main heat that caused the beginning of the 2020 melting season. A very interesting phenomenon is that the SWSD in both May 2019 and May 2020 showed obvious positive anomalies, but SWN was the only clear positive anomaly in May 2019 (Figures 4B,D,F). Therefore, the heat of SWN in spring is also another reason for 1) and 2) mentioned above.

In addition, at the beginning of the melting season in 2019 (mid–May to mid–June), the SIC fluctuated within a small range. This may have been due to the negative anomalies of LWN from mid–to–late April to early June 2019 (Figure 3 and Figure 4A).

This change in the surface flux is related to the abnormal changes in cloud water and water vapor, as well as convergence and divergence. The water vapor content in the study area from April to June 2019 in spring was almost all abnormally high, and the change in the trend of the cloud water content was almost the same as that of LWN (Figure 5A). The latent heat–transport convergence showed significant positive anomalies in May and June, which is conducive to moisture increase (Graversen, Mauritsen, Drijfhout, Tjernström, and Mårtensson, 2011) (Figure 5B). The cloud water and water vapor, which are higher than average, will increase the opacity of the atmosphere, thereby causing the greenhouse effect, which leads to an increase in LWN (Kapsch, Graversen, Tjernström, and Bintanja, 2016; Mortin, Svensson, Graversen, Kapsch, Stroeve, and Boisvert, 2016; Lee, Kwon, Yeh, Kwon, Park, Park et al., 2017; Gimeno, Vázquez, Eiras-Barca, Sorí, Algarra, and Nieto, 2019; He, Hu, Chen, Wang, Huang, and Stamnes, 2019). The reason for the abnormally low LWN in May is mainly related to the abnormally low cloud water, and has nothing to do with water vapor and the latent heat–transport convergence (Figures 5A,B). In April–May 2020, although the latent heat–transport convergence showed a positive anomaly, the changes in cloud water and water vapor were small enough to result in relatively weak LWN and LH variability (Figures 5C,D). In June, the abnormal change of water vapor was very small, and the latent heat–transport divergence, the positive anomalies of LWN and LH were mainly caused by the positive anomalies of water vapor (Figures 5C,D).

In the previous analysis, we found that in May 2019 and May 2020, when the SWSD anomalies were both positive, SWN showed positive anomalies in 2019 but negative ones in 2020. Comparing Figures 5A,C,E, the abnormally high SWN in May 2019 is closely related to the abnormally low total column cloud water. The presence of clouds can absorb part of the solar radiation and reflect some of it into the atmosphere, and its abnormal reduction can inhibit the formation of clouds, thereby increasing the shortwave radiation absorbed by the surface (Kay et al., 2008; Barrientos Velasco, Deneke, Griesche, Seifert, Engelmann, and Macke, 2020; Liang, Bi, Wang, Zhang, and Huang, 2020).

In addition to the abnormal changes in moisture, the convergence and divergence of energy also affect the changes

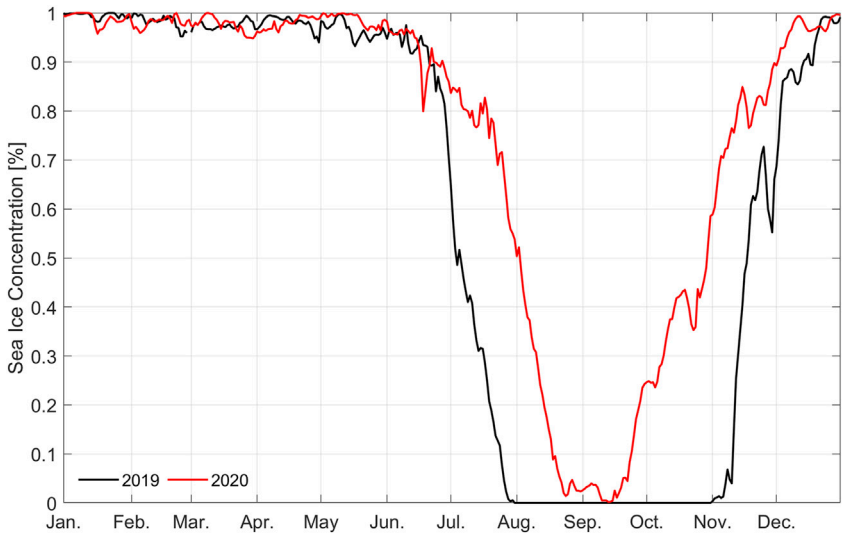

FIGURE 3
Regional average (73–75°N and 168–150°W) daily SIC for 2019 (black) and 2020 (red) based on satellite observation data.

of LWN, which is characterized by the convergence of the dry–static transport in this paper. The positive anomaly of the dry–static transport convergence in April and June 2019 is favorable to the appearance of positive anomalies in LWN (Figures 5B,F). The occurrence of negative anomalies of LWN in May also be related to the negative anomalies of dry–static transport convergence (Figures 5B,F). The change in dry–static transport convergence in the spring of 2020 had little effect on the LWN changes (Figures 5D,F).

In 2019, SWN began to show positive anomalies and gradually increased from mid–July, while SWSD displayed negative anomalies in July (Figures 4A,B). The reasons are as follows. First, there is less sea ice and less solar radiation reflected back. The reflection of sea ice is crucial to the absorption of solar shortwave radiation (Landy, Ehn, and Barber, 2015; Gong, Feldstein, and Lee, 2017). Second, the positive anomaly trend of the total column cloud water was declining, indicating that it is crucial to solar radiation in summer (Figure 5A). The trend of SWN showing a negative anomaly and gradually increasing in July 2020 may be related to the positive anomaly of cloud water and its increasing trend.

Across the surface, the energy balance is given by

$$F_{srf} = SWN + LWN + SH + LH \tag{1}$$

that is, the sum of net shortwave radiation, net longwave radiation, sensible flux and latent flux (Kapsch, Graversen, and Tjernström, 2013; Bintanja and Krikken, 2016; Liu, Chen, Francis, Song, Mote, and Hu, 2016). All terms in Equation 1 are defined positive downward.

Sea ice melted by the extra heat gained by the surface is given by

$$\Delta F_{srf} \times t \Big/ L_f \Big/ \rho_{ice} \tag{2}$$

t is set to 91 days (total number of days from April to June), $L_f = 334 \times 10^3\ J \cdot kg^{-1}$ is the latent heat of fusion, and $\rho_{ice} = 900\ kg \cdot m^{-3}$ is sea ice density (Kapsch, Graversen, and Tjernström, 2013).

By the end of spring (end of June), the SIC in 2019 dropped below 60%, whereas in 2020 it was around 85%. During April–June 2019 and 2020, there was a total energy surplus of ~6.87 $W \cdot m^{-2}$ and ~4.36 $W \cdot m^{-2}$ over the study area per day, respectively (Table 1). The extra energy gained by the surface due to these anomalies can melt on average ~18 cm and ~11 cm of ice over the area during spring. The ΔF_{srf} anomalies in 2019 mainly resulted from LWN, SH and SWN. The positive anomaly of SH may have been caused by the temperature difference between the surface of the ocean and sea ice and the bottom of the atmosphere. The ΔF_{srf} anomalies in 2020 mainly originated from LWN and LH. The heat accumulated in the spring (April to June) will affect the start time of the melting season on the one hand. On the other hand, as more and more multi–year ice has changed into first–year ice in recent years, especially after 2000s, the divergence of ice caused by ice movement in spring lays the foundation for the strengthening of the positive feedback of solar radiation–albedo in summer (Kapsch, Graversen, and Tjernström, 2013; Kashiwase, Ohshima, Nihashi, and Eicken, 2017).

On the basis of the current state of sea ice at the end of spring, more open sea areas have strengthened the positive albedo feedback. In July 2019, the daily positive SWN anomaly

FIGURE 4
Radiative and turbulent flux anomalies at the surface for 2019 [top, **(A,B)**], 2020 [middle, **(C,D)**] and 2020 minus 2019 [bottom, **(E,F)**] using method one. The black line shows the SIC (right−hand axis). **(A,C,E)**, the latent flux (LH; blue), the sensible flux (SH, pink), the net shortwave radiation (SWN; green) and the net longwave radiation (LWN; red). **(B,D,F)**, downwelling longwave (LWSD; red) and shortwave (SWSD; green) radiation. All time series are averaged over the area 73–75°N by 168–150°W.

reached 11.9 $W \cdot m^{-2}$ and by the end of July, the SIC had reached 0 (Table 1). In contrast, there was no positive solar radiation anomaly in July 2020, and the SIC reduced to about 50% at the end of July.

Park et al. (2015), Lee et al. (2017) and Gimeno et al. (2019) found that moisture from low latitudes, rather than local water vapor, is the main cause of abnormal LWN (Park, Lee, Son, Feldstein, and Kosaka, 2015; Lee, Kwon, Yeh, Kwon, Park, Park et al., 2017; Gimeno, Vázquez, Eiras-Barca, Sorí, Algarra, and Nieto, 2019). In this study, we found that in July 2019, the heat flux (Figure 6A), the water vapor flux (Figure 6C) and the cloud liquid water flux (Figure 6E) in the southern Northwind Ridge all showed strong poleward transport from south to north; whereas in July 2020, the three fluxes had southward transport (Figures 6B,D,F). This difference indicates that not only moisture, but also heat at low latitudes, contribute significantly to the anomalous sea ice changes on the southern Northwind Ridge.

Compared with 2020, the strengthening of the warm and humid advection from the low latitudes at the southern Northwind Ridge in July 2019 was mainly caused by an abnormal pressure field, which can excite anomalous winds (Wei, Qin, and Li, 2017; Gimeno, Vázquez, Eiras-Barca, Sorí, Algarra, and Nieto, 2019). On the MSLP field (Figure 6 and Supplementary Figure S6), the centers of low MSLP and high

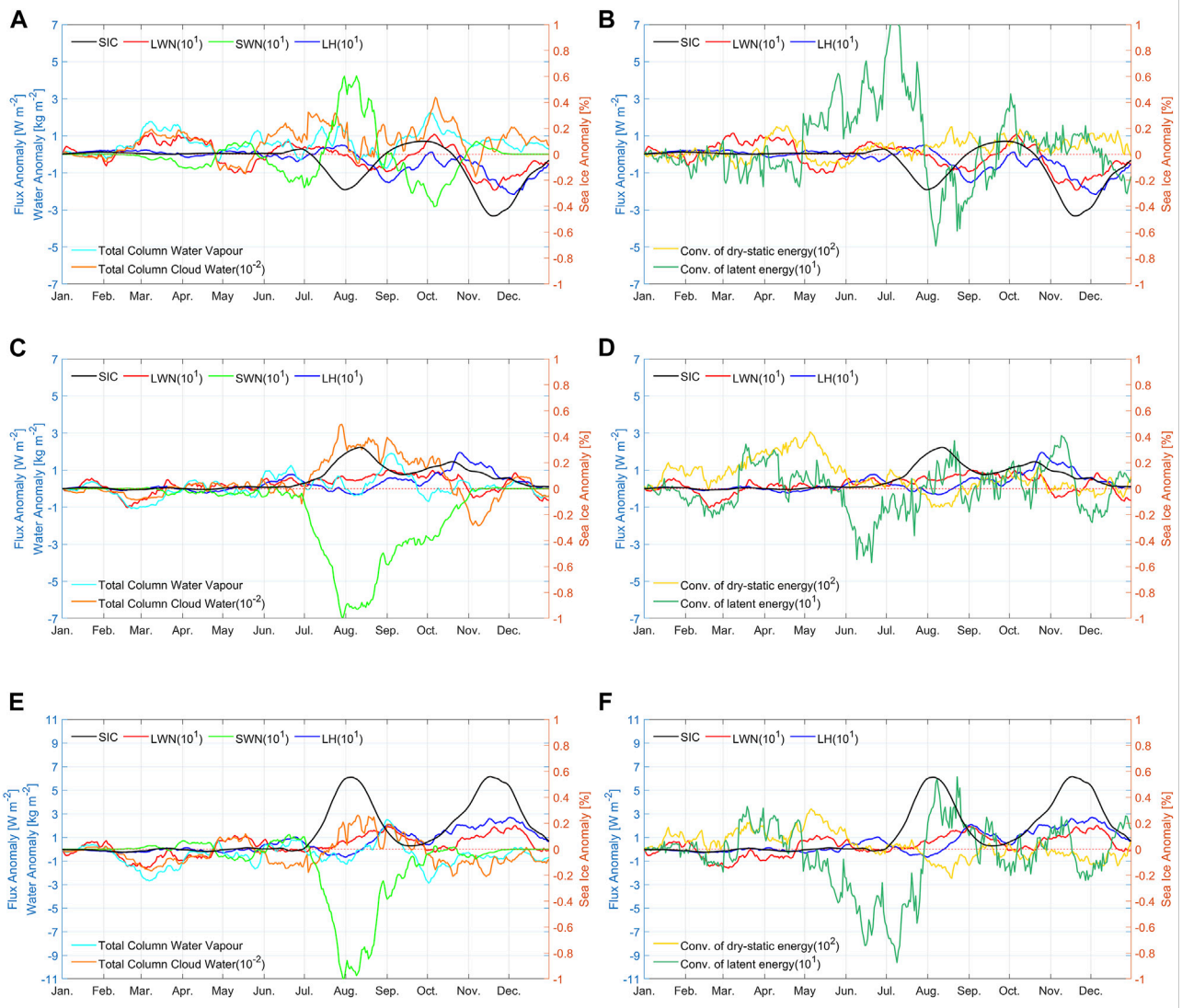

FIGURE 5
Atmospheric water content and energy convergence anomalies for 2019 [top, **(A,B)**], 2020 [middle, **(C,D)**] and 2020 minus 2019 [bottom, **(E,F)**] using method one. The black line shows the SIC (right–hand axis). **(A,C,E)**, the net longwave radiation (red), the net shortwave radiation (green) and latent flux (blue) are shown together with the anomalies of total column cloud water (liquid plus solid; orange) and water vapor (celeste), **(B,D,F)**, as well as the convergence of dry-static (gold) and latent atmospheric energy transport (prasinous).

TABLE 1 The daily positive anomalies of surface fluxes in the spring (May to June) and July of 2019 and 2020. All fields are averaged over the study area and over the selected time periods (units: $W \times m^{-2}$).

	spring in 2019 (%)	spring in 2020 (%)	July in 2019 (%)	July in 2020 (%)
SWN	1.41 (20.5%)	0.05 (1.1%)	11.90 (62.3%)	0
LWN	3.19 (46.4%)	2.03 (46.6%)	2.43 (12.7%)	4.51 (83.1%)
LH	0.46 (6.7%)	1.88 (43.1%)	2.66 (13.9%)	0.91 (16.8%)
SH	1.82 (26.5%)	0.41 (9.4%)	2.12 (11.1%)	0
Total	6.87	4.36	19.11	5.43

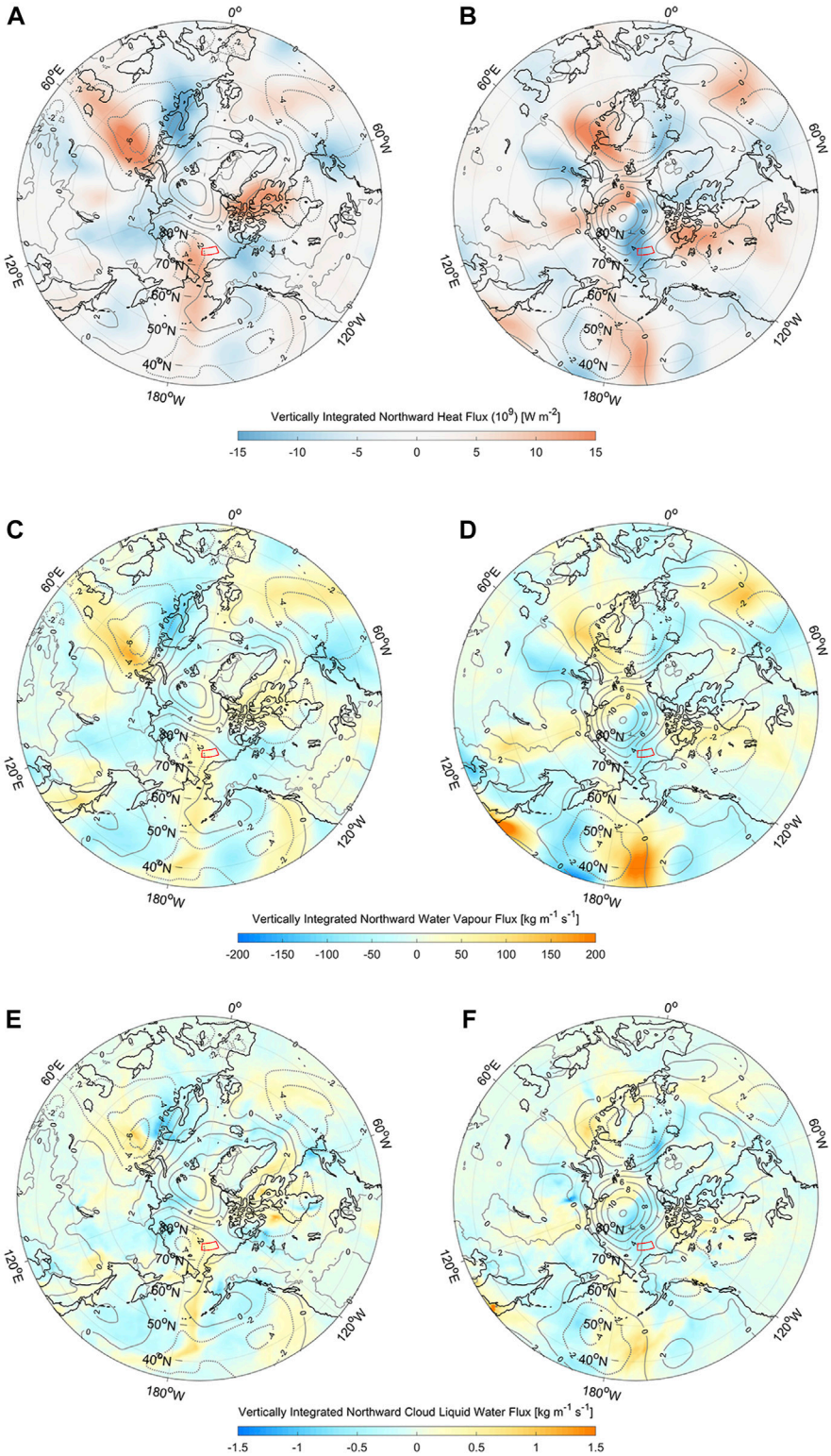

FIGURE 6
The MSLP anomaly field (contour, the solid gray line is the positive anomaly, the gray dashed line is the negative anomaly) in July 2019 **(A,C,E)** and July 2020 **(B,D,F)** superimposed on the anomaly of the vertically integrated northward heat flux **(A,B)**, vertically integrated northward water vapor flux **(C,D)** and the vertically integrated northward cloud liquid water flux **(E,F)**. Red polygons encapsulate areas represents the study area of this paper.

MSLP in the Arctic Ocean intersected near 84°N in July 2019. As the low–pressure center rotates counterclockwise and the high–pressure center rotates clockwise, the 10 m wind near the southern Northwind Ridge is southerly as a whole, and the wind speed increases correspondingly due to the influence of the intersection of the two pressure centers (Figure 7A). The strengthening of warm and humid advection brings more heat and moisture, which will on the one hand increase longwave radiation, latent heat flux, and sensible heat flux; and on the other hand, affect solar radiation by affecting cloud formation, influencing the melting of sea ice. The MSLP at this time (July 2019) was similar to the positive phase of the Arctic dipole (AD; a persistent pattern of pressure characterized by high pressure in the Beaufort Sea region and low pressure in the Arctic region of Siberia). In July 2020, most of the Arctic Ocean was dominated by the high MSLP center, the wind field was generally northerly, and the wind speed was greatly reduced (Figure 7B). The MSLP was similar to the negative phase of the Arctic oscillation (AO), which is characterized by positive geopotential height over the Arctic, and the heat and moisture transfer are reduced (Wang and Su, 2019).

In addition to the MSLP field, we found that there was appeared to be a positive pattern similar to the Pacific North American (PNA) pattern at the 500 hPa level in June 2019, expressed as an anomalous anticyclone over the western Arctic (Liu, Risi, Codron, He, Poulsen, Wei et al., 2021) (Supplementary Figure S7). This is beneficial to the heat and moisture transport from the North Pacific into the western Arctic in July (Liu, Risi, Codron, He, Poulsen, Wei et al., 2021) (Supplementary Figure S7). In June 2020, the PNA had a negative anomaly.

Compared with July 2020, the wind speed near the southern Northwind Ridge increased by nearly 2 $m \cdot s^{-1}$ in July 2019. In the atmosphere, the enhanced 10 m wind field can enhance the vertical mixing, pulling down warm air from the upper layer, and increase the sensible heat flux. For sea ice, higher wind speeds are more conducive to the movement of sea ice, especially in summer when sea ice is thinner and more sparse (Liang, Bi, Wang, Zhang, and Huang, 2020). In the ocean, sea surface wind can also weaken the stability of the upper ocean and increase turbulence. The results indicate that the thermodynamical and dynamical processes are probably linked, because the positive anomalies of energy convergence are associated with cyclone and frontal activities and enhanced winds.

Discussion

On the southern Northwind Ridge in the Arctic, which experiences extensive sea ice changes, the maximum and second minimum years of SIC were 2020 and 2019, respectively, after the removal of the long–term trend of July from 1979 to 2020. Furthermore, the difference in the SIC anomalies between the 2 years reached 45% (Figure 2B). This paper uses various atmospheric fields from ERA5 to explore the main reasons for the abnormally low sea ice in 2019, the abnormally high sea ice in 2020 and the difference between the 2 years by applying a detrending method and an improved averaging method.

We found that the main radiation factor influencing the sea ice in July is solar radiation. The positive SWN anomaly in July 2019 and the negative SWN anomaly in July 2020 are both closely related to cloud water and albedo. In 2019, a sharp downward

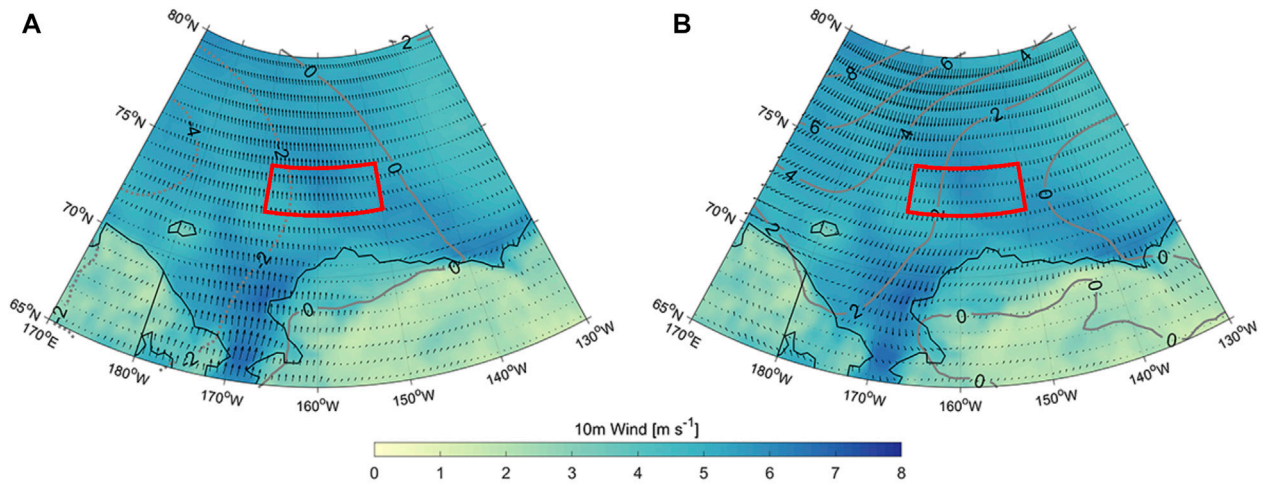

FIGURE 7
The MSLP anomaly field (contour, the solid gray line is the positive anomaly, the gray dashed line is the negative anomaly) in July 2019 **(A)** and July 2020 **(B)** superimposed on the 10 m wind field. The coloring shows the value of the wind field and the arrows indicate the direction. Red polygons encapsulate areas represents the study area of this paper.

trend in sea ice began in mid–June, which was much larger than the change in sea ice in 2020. This difference directly affects the base of SIC in July, and will change the effect of the radiation flux in July on sea ice by affecting the positive radiation–albedo feedback. For this reason, we studied the surface radiation fluxes in spring one by one, including LWN, SWN, LH and SH, which affect the changes in sea ice from mid–June to the beginning of the ice melting season. Compared with 2020, the convergence of moisture and the positive anomalies of cloud water and water vapor in 2019 during the spring period contributed to the increase of LH on the one hand, and the increase LWN through the greenhouse effect on the other. In addition, the convergence of energy was also conducive to the enhancement of LWN. SH was mainly related to the temperature difference between the atmosphere and the ocean or sea ice. It is worth noting that the lack of cloud water inhibited the formation of clouds resulting in an abnormal increase in SWN in May 2019, which is the main source of energy surplus in the spring of 2019. We also found that the positive phase of AD–like in the MSLP field in July and the positive phase of the PNA–like in the 500 hPa geopotential height field in June, which transported moisture and heat northward, made major contributions to the anomalous surface radiant flux.

We analyzed the reasons for the large difference in the SIC between July 2019 and July 2020 for spring (April–June) and July. The extra energy gained by the surface due to radiative flux anomalies in spring could have melted on average ~18 cm of ice in 2019 and ~11 cm in 2020 over the southern Northwind Ridge. Among the four surface radiative fluxes (LWN, SWN, LH and SH), the positive SWN anomalies in May 2019 were the main contributor. The positive SWN anomaly in 2019 for July reached 11.9 $W \cdot m^{-2}$ per day.

However, we mainly discuss the reasons for the abnormal sea ice changes from the thermal aspect. It is also mentioned that in July, dynamic factors may also be a major reason for the abnormal sea ice changes, such as sea ice deformation or sea ice output (Lei, Tian-Kunze, Li, Heil, Wang, Zeng et al., 2017a). In addition, the melting of ice bottom caused by enhanced release of oceanic heat has at a rate now comparable to losses from atmospheric thermodynamic forcing (Polyakov, Timokhov, Alexeev, Bacon, Dmitrenko, Fortier et al., 2010; Lin and Zhao, 2019; Wang, Liu, and Zhang, 2021). Both dynamic factors and ocean changes need to be further analyzed and improved in subsequent studies.

Data availability statement

The original contributions presented in the study are included in the article/Supplementary Material, further inquiries can be directed to the corresponding author.

Author contributions

LX wrote the paper; LNa funded and revised the paper; LL revised the introduction and format; YL revised the paper; LY and FL revised the format; CH revised formula; WY and KB came up with creative ideas; ZY and LNi embellished figures. All authors have read and agreed to the published version of the manuscript.

Funding

This research was funded by Global Change and Air–Sea Interaction II (Grant No. ZY0720032/ZY0721015), National key research and development program (Grant No. 2019YFC1509101), National Natural Science Foundation of China under contact Nos. 42106232, 42106230, and 41806214, "Arctic Drifting Ice Camp Project (MOSAiC Project) in 2020" and Ministry of Science and Technology of China under contact No. 2019YFC1408201.

Acknowledgments

Thanks for the comments and carefulness of the reviewers and editors. We also thank International Science Editing (http://www.internationalscienceediting.com) for editing this manuscript.

Conflict of interest

The authors declare that the research was conducted in the absence of any commercial or financial relationships that could be construed as a potential conflict of interest.

Publisher's note

Supplementary material

The Supplementary Material for this article can be found online at: https://www.frontiersin.org/articles/10.3389/feart.2022.993074/full#supplementary-material

References

Barrientos Velasco, C., Deneke, H., Griesche, H., Seifert, P., Engelmann, R., and Macke, A. (2020). Spatiotemporal variability of solar radiation introduced by clouds over arctic sea ice. *Atmos. Meas. Tech.* 13, 1757–1775. doi:10.5194/amt-13-1757-2020

Bintanja, R., and Krikken, F. (2016). Magnitude and pattern of arctic warming governed by the seasonality of radiative forcing. *Sci. Rep.* 6, 38287–7. doi:10.1038/srep38287

Cox, C. J., Walden, V. P., and Rowe, P. M. (2012). A comparison of the atmospheric conditions at eureka, Canada, and barrow, Alaska (2006–2008). *J. Geophys. Res.* 117, 017164. doi:10.1029/2011jd017164

Curry, J. A., Schramm, J. L., and Ebert, E. E. (1995). Sea ice-albedo climate feedback mechanism. *J. Clim.* 8, 240–247. doi:10.1175/1520-0442(1995)008<0240:siacfm>2.0.co;2

Danielson, S., Ahkinga, O., Ashjian, C., Basyuk, E., Cooper, L., Eisner, L., et al. (2020). Manifestation and consequences of warming and altered heat fluxes over the bering and chukchi sea continental shelves. *Deep Sea Res. Part II Top. Stud. Oceanogr.* 177, 104781. doi:10.1016/j.dsr2.2020.104781

Gimeno, L., Vázquez, M., Eiras-Barca, J., Sorí, R., Algarra, I., and Nieto, R. (2019). Atmospheric moisture transport and the decline in arctic sea ice. *WIREs Clim. Change* 10, e588. doi:10.1002/wcc.588

Gong, T., Feldstein, S., and Lee, S. (2017). The role of downward infrared radiation in the recent arctic winter warming trend. *J. Clim.* 30, 4937–4949. doi:10.1175/jcli-d-16-0180.1

Graversen, R. G. (2006). Do changes in the midlatitude circulation have any impact on the arctic surface air temperature trend? *J. Clim.* 19, 5422–5438. doi:10.1175/jcli3906.1

Graversen, R. G., Mauritsen, T., Drijfhout, S., Tjernström, M., and Mårtensson, S. (2011). Warm winds from the pacific caused extensive arctic sea-ice melt in summer 2007. *Clim. Dyn.* 36, 2103–2112. doi:10.1007/s00382-010-0809-z

Graversen, R. G., Mauritsen, T., Tjernström, M., Källén, E., and Svensson, G. (2008). Vertical structure of recent arctic warming. *Nature* 451, 53–56. doi:10.1038/nature06502

Haiden, T., Janousek, M., Vitart, F., Ben-Bouallegue, Z., Ferranti, L., Prates, C., et al. (2021). Evaluation of ecmwf forecasts, including the 2020 upgrade doi:10.21957/6njp8byz4

He, M., Hu, Y., Chen, N., Wang, D., Huang, J., and Stamnes, K. (2019). High cloud coverage over melted areas dominates the impact of clouds on the albedo feedback in the arctic. *Sci. Rep.* 9, 9529–9611. doi:10.1038/s41598-019-44155-w

Hersbach, H., Bell, B., Berrisford, P., Biavati, G., Horányi, A., Muñoz Sabater, J., et al. (2018). *Era5 hourly data on single levels from 1979 to present*. ECMWF Reading, United Kingdom: copernicus climate change service (c3s) climate data store. (cds).

Kapsch, M.-L., Graversen, R. G., Tjernström, M., and Bintanja, R. (2016). The effect of downwelling longwave and shortwave radiation on arctic summer sea ice. *J. Clim.* 29, 1143–1159. doi:10.1175/JCLI-D-15-0238.1

Kapsch, M.-L., Graversen, R. G., and Tjernström, M. (2013). Springtime atmospheric energy transport and the control of arctic summer sea-ice extent. *Nat. Clim. Chang.* 3, 744–748. doi:10.1038/nclimate1884

Kashiwase, H., Ohshima, K. I., Nihashi, S., and Eicken, H. (2017). Evidence for ice-ocean albedo feedback in the arctic ocean shifting to a seasonal ice zone. *Sci. Rep.* 7, 8170–8210. doi:10.1038/s41598-017-08467-z

Kay, J. E., L"Ecuyer, T., Gettelman, A., Stephens, G., and O"Dell, C. (2008). The contribution of cloud and radiation anomalies to the 2007 arctic sea ice extent minimum. *Geophys. Res. Lett.* 35, 085033–L9202. doi:10.1029/2008gl033451

Landy, J. C., Ehn, J. K., and Barber, D. G. (2015). Albedo feedback enhanced by smoother arctic sea ice. *Geophys. Res. Lett.* 42, 714–720. doi:10.1002/2015gl066712

Lee, H., Kwon, M., Yeh, S.-W., Kwon, Y.-O., Park, W., Park, J.-H., et al. (2017). Impact of poleward moisture transport from the north pacific on the acceleration of sea ice loss in the arctic since 2002. *J. Clim.* 30, 6757–6769. doi:10.1175/jcli-d-16-0461.1

Lei, R., Tian-Kunze, X., Li, B., Heil, P., Wang, J., Zeng, J., et al. (2017a). Characterization of summer arctic sea ice morphology in the 135–175 w sector using multi-scale methods. *Cold Regions Sci. Technol.* 133, 108–120. doi:10.1016/j.coldregions.2016.10.009

Lei, R., Zhang, Z., Li, Z., Yang, Q., Li, B., and Li, T. (2017b). Review of research on arctic sea ice physics based on the Chinese national arctic research expedition. *Adv. Polar Sci.* 28, 100–110.

Liang, Y., Bi, H., Wang, Y., Zhang, Z., and Huang, H. (2020). Role of atmospheric factors in forcing arctic sea ice variability. *Acta Oceanol. Sin.* 39, 60–72. doi:10.1007/s13131-020-1629-6

Lin, L., and Zhao, J. (2019). Estimation of oceanic heat flux under sea ice in the arctic ocean. *J. Ocean. Univ. China* 18, 605–614. doi:10.1007/s11802-019-3877-7

Liu, J., Chen, Z., Francis, J., Song, M., Mote, T., and Hu, Y. (2016). Has arctic sea ice loss contributed to increased surface melting of the Greenland ice sheet? *J. Clim.* 29, 3373–3386. doi:10.1175/jcli-d-15-0391.1

Liu, Z., Risi, C., Codron, F., He, X., Poulsen, C. J., Wei, Z., et al. (2021). Acceleration of western arctic sea ice loss linked to the pacific north american pattern. *Nat. Commun.* 12, 1519–9. doi:10.1038/s41467-021-21830-z

Mizobata, K., and Shimada, K. (2012). East–west asymmetry in surface mixed layer and ocean heat content in the pacific sector of the arctic ocean derived from amsr-e sea surface temperature. *Deep Sea Res. Part II Top. Stud. Oceanogr.* 77, 62–69. doi:10.1016/j.dsr2.2012.04.005

Mortin, J., Svensson, G., Graversen, R. G., Kapsch, M.-L., Stroeve, J. C., and Boisvert, L. N. (2016). Melt onset over arctic sea ice controlled by atmospheric moisture transport. *Geophys. Res. Lett.* 43, 6636–6642. doi:10.1002/2016gl069330

Park, H.-S., Lee, S., Son, S.-W., Feldstein, S. B., and Kosaka, Y. (2015). The impact of poleward moisture and sensible heat flux on arctic winter sea ice variability. *J. Clim.* 28, 5030–5040. doi:10.1175/jcli-d-15-0074.1

Polyakov, I. V., Beszczynska, A., Carmack, E. C., Dmitrenko, I. A., Fahrbach, E., Frolov, I. E., et al. (2005). One more step toward a warmer arctic. *Geophys. Res. Lett.* 32. doi:10.1029/2005gl023740

Polyakov, I. V., Timokhov, L. A., Alexeev, V. A., Bacon, S., Dmitrenko, I. A., Fortier, L., et al. (2010). Arctic ocean warming contributes to reduced polar ice cap. *J. Phys. Oceanogr.* 40, 2743–2756. doi:10.1175/2010jpo4339.1

Shi, X., Wild, M., and Lettenmaier, D. P. (2010). Surface radiative fluxes over the pan-arctic land region: Variability and trends. *J. Geophys. Res.* 115, D22104. doi:10.1029/2010jd014402

Sumata, H., and Shimada, K. (2007). Northward transport of pacific summer water along the northwind ridge in the western arctic ocean. *J. Oceanogr.* 63, 363–378. doi:10.1007/s10872-007-0035-4

Wang, S., and Su, J. (2019). Numerical simulation of the effects of arctic dipole atmospheric circulation on arctic sea ice. *Clim. Change Res. Lett.* 08, 503–515. doi:10.12677/CCRL.2019.84055

Wang, Y., Liu, N., and Zhang, Z. (2021). Sea ice reduction during winter of 2017 due to oceanic heat supplied by pacific water in the chukchi sea, west arctic ocean. *Front. Mar. Sci.* 595. doi:10.3389/fmars.2021.650909

Wei, L., Qin, T., and Li, C. (2017). Seasonal and inter-annual variations of arctic cyclones and their linkage with arctic sea ice and atmospheric teleconnections. *Acta Oceanol. Sin.* 36, 1–7. doi:10.1007/s13131-017-1117-9

Wu, B., Zhang, R., Wang, B., and D'Arrigo, R. (2009). On the association between spring arctic sea ice concentration and Chinese summer rainfall. *Geophys. Res. Lett.* 36, L09501. doi:10.1029/2009gl037299

Zygmuntowska, M., Mauritsen, T., Quaas, J., and Kaleschke, L. (2012). Arctic clouds and surface radiation–a critical comparison of satellite retrievals and the era-interim reanalysis. *Atmos. Chem. Phys.* 12, 6667–6677. doi:10.5194/acp-12-6667-2012